Available online at www.sciencedirect.com
SCIENCE DIRECT®
Journal of Catalysis 222 (2004) 53–64
JOURNAL OF CATALYSIS
www.elsevier.com/locate/jcat

The vanadium subsurface alloy on polycrystalline rhodium: formation and catalytic properties

Wolfgang Reichl [1] and Konrad Hayek *

Institut für Physikalische Chemie, Leopold-Franzens-Universität Innsbruck, Innrain 52a, A-6020 Innsbruck, Austria

Received 20 June 2003; revised 23 August 2003; accepted 10 September 2003

Abstract

Stable vanadium/rhodium subsurface alloys can be obtained by annealing vanadium metal overlayers on polycrystalline rhodium at elevated temperatures ($\geqslant$ 773 K). Their peculiarity is a purely rhodium-terminated surface with vanadium atoms positioned in the near-surface layers. Their structure and composition depend on the nominal vanadium coverage and on the sample temperature during preparation. In the present contribution the formation of the vanadium/rhodium subsurface alloy was studied in detail and the kinetics of CO hydrogenation on its surface was measured in situ at the different stages of alloy formation. In particular, the transition from "on-top" vanadium to the subsurface alloy state and finally to the bulk solution has been monitored with the help of Auger electron spectroscopy and argon ion sputter profiling. Submonolayers of vanadium *on top of* the rhodium surface promote initially the CO hydrogenation, but are rapidly deactivated by oxide and carbide formation. Subsurface alloy formation sets in upon annealing at 773 K and is connected with a significant increase of the catalytic activity, a change in the selectivity, and a reduced catalyst deactivation. Increasing the annealing temperature to 950 K leads to a state with the subsurface layer (second Rh surface layer) saturated with vanadium and excess vanadium dissolved into the bulk. The formation and the catalytic properties of the (sub)surface alloys obtained at different temperatures are discussed in light of additional experiments regarding their chemisorptive properties and of recent theoretical calculations.
© 2003 Elsevier Inc. All rights reserved.

Keywords: V–Rh subsurface alloy; Rhodium; Vanadium; CO hydrogenation; Inverse model catalyst; Metal–support interaction; Auger electron spectroscopy; Argon ion sputtering

1. Introduction

During the last decades the chemical industry has increasingly benefited from the catalytic properties of bimetallic systems. The recent development of experimental and theoretical tools has allowed study of alloy surfaces on an atomic scale and correlation of structural and electronic properties with catalytic performance. A great number of studies have been compiled in extensive reviews [1–5] and most of them have emphasized the role of structural (ensemble) and electronic (ligand) effects in bimetallic catalysis. While ensemble effects can be described in terms of the number of neighboring sites required for a reaction to occur, ligand effects are a result of electronic interaction and transfer of charge between the two components. Due to their simultaneous occurrence their discrimination is usually difficult. It is, however, feasible on a number of newly described subsurface alloys in which the surface is purely noble metal terminated and the second metal is positioned in the lower layers.

Subsurface alloys like V/Pd [6,7] and V/Rh [8–10] are easily prepared by depositing small amounts of the "early" transition metal on the (single-crystal or polycrystalline) surface of the "late" transition metal and subsequent annealing. The noble metal skin provides a uniform composition of the topmost surface layer and excludes conventional ensemble effects. The strong chemical interaction between the two dissimilar atoms accounts for a high thermal stability of the second layer, which in turn influences the catalytic properties of the topmost layer via pure ligand effects. The modification of the subsurface layer with a different metal is therefore an interesting approach to improve the catalytic properties of a metal surface.

In a recent study of a subsurface alloy prepared from vanadium on polycrystalline rhodium [10] we were able to show that the activity of the Rh surface for CO hydrogena-

* Corresponding author.
E-mail address: konrad.hayek@uibk.ac.at (K. Hayek).
[1] Present address: E+E Elektronik GmbH, A-4209 Engerwitzdorf, Austria.

0021-9517/$ – see front matter © 2003 Elsevier Inc. All rights reserved.
doi:10.1016/j.jcat.2003.09.019

tion can be reproducibly controlled by the initial vanadium metal loading and the temperature of annealing, both determining the vanadium content of the subsurface layers. It could also be shown that the subsurface alloy state is also reached by a high-temperature hydrogen treatment of vanadia submonolayers on Rh. These overlayers are known to promote the catalytic activity of a Rh surface like other reducible oxides and to change the selectivity toward longer chain hydrocarbons [11,12], but after high-temperature reduction they exhibit the characteristic catalytic properties of the subsurface alloy [10].

In order to understand the catalytic properties of surface and subsurface alloys of V/Rh in detail it is necessary to know the composition and structure of the surface and subsurface layers as a function of the preparation conditions. In contrast to experiments on single crystal surfaces where both the growth of the overlayer containing the second metal and its transition to the subsurface alloy state are accessible by scanning tunneling microscopy (STM) [6,8], studies on polycrystalline substrates are only feasible by the extensive use of Auger electron spectroscopy and related techniques. In the present paper we describe the transition from the as-grown vanadium/rhodium system (vanadium "on-top") to the subsurface alloy state and finally to the solution of vanadium in the rhodium bulk. This knowledge will allow a better correlation of the composition and structure of the (sub)surface layers with the corresponding changes in activity, selectivity, and catalyst deactivation.

2. Experimental

The experimental setup was described in detail previously [13]. A Pyrex glass reactor of the batch recirculation type (high-pressure cell, HPC) is connected to an ultrahigh vacuum (UHV) chamber via a sample transfer port. The UHV chamber is organized in two levels: The upper level is equipped with an Auger electron spectrometer (AES, CMA from Staib Instruments), an ion sputter gun, and a linear transfer unit. The lower level holds two electron beam evaporators, two quartz crystal microbalances, and an electron beam heater. Gases are introduced into the chamber via a dosing manifold and the residual gas composition is monitored with a mass spectrometer. A turbomolecular pump evacuates the chamber to a base pressure in the low 10^{-10} mbar range. In the UHV chamber the samples (thin metal foils, size 4 cm^2) are handled by a long z-travel $xyz\varphi$-manipulator. For transfer from UHV into the reaction cell the sample is detached from the manipulator and placed in a Pyrex glass frame mounted on a transfer car, which is then moved into the reaction cell without breaking the vacuum. The cell is sealed by a special mechanism described in [13] and pressurized up to 2 bar. The design of the system allows the preparation of both sample faces, resulting in a high catalyst surface area (8 cm^2) to the benefit of the kinetic experiments.

The reaction gases are premixed and introduced via a gas-handling manifold. A recirculation pump, a pressure gauge, and a sample valve are connected to the reactor circulation system and the reactor is heated by an external oven. Since both the reactor cell and the sample holder consist of glass no other metal parts such as connecting wires and holders are exposed to the reacting gas.

A polycrystalline rhodium foil (Goodfellow, 99.9% purity, thickness 0.125 mm) was cleaned in UHV by cycles of argon ion sputtering (500 eV), heating in oxygen (2.0×10^{-7} mbar, $\leqslant 1000$ K) and hydrogen (2.0×10^{-7} mbar, $\leqslant 673$ K), and annealing in vacuum until no impurities were detected. Every further preparation step and the state before and after catalytic reactions were also monitored by AES.

Vanadium overlayers were prepared by electron beam evaporation of the metal from a 1-mm rod (Goodfellow, 99.996% purity). During deposition the sample was at room temperature and the residual gas pressure was below 8×10^{-10} mbar. The deposition rate was monitored by a calibrated quartz microbalance and was typically about 0.3 monolayers (ML)/min. The V coverage is given in monolayer equivalents (ML). A 1 ML V on polycrystalline Rh is defined as a vanadium atom density of 1.5×10^{15} atoms/cm^2 (average of close packed Rh(111) and Rh(100) facets). The deposited vanadium layers were free of contamination as checked by AES. Subsequent annealing was preferably performed in a hydrogen atmosphere (up to 2.0×10^{-7} mbar H_2) in order to avoid, respectively to remove, carbon and oxygen contamination. The samples were annealed at a given temperature (473–1050 K) for 10 min. Control experiments showed that longer heating times did not induce any additional changes below 670 K and above 870 K, but in the "dynamic" temperature range between 670 and 870 K changes of the relevant V and Rh Auger signals were still observed upon extending the heating time to 30 min.

The composition of surface and subsurface layers is most conveniently studied with Auger electron spectroscopy in combination with argon ion sputter profiling. The profiles were obtained from the changes of the respective Auger signals after consecutive sputtering steps under identical conditions. The operation parameters of the sputter gun and the sample sputter gun geometry were also identical in all experiments. The incidence angle of the argon beam was 90° with respect to the surface and the acceleration voltage was 500 V. At an Ar pressure of approximately 5×10^{-5} mbar the sample current was 0.65 ± 0.02 μA. AES spectra were taken in regular time intervals, always on the same spot on each sample.

The kinetics of CO hydrogenation was studied usually at 573 K under varying reactant pressures. Samples were taken periodically and analyzed by gas chromatography with mass-selective detection. The initial reaction rates were determined from conversion versus time plots. The measured reaction rates were reproducible within 5% so that the kinetic data obtained under specified conditions could be used, in addition to AES, as a proof for sample

cleanliness. The turnover frequency (TOF) was calculated with respect to the geometric area of the rhodium substrate (1.5×10^{15} atoms/cm^2). Vanadium overlayers and the V/Rh subsurface alloy could be removed from the surface by consecutive cycles of oxidation (2.0×10^{-7} mbar O_2 at 673 K for 10 min) and Ar-ion sputtering, followed by reduction (2.0×10^{-7} mbar H_2 at 673 K for 10 min). This procedure was repeated until no impurity, in particular no residual V, was detected by AES. In addition, the activity of the sample was determined and compared to the "standard" activity of the pristine clean Rh surface (measured at 40 mbar CO, 360 mbar H_2, 600 mbar He, 573 K) in order to assure the reproducibility of the kinetic measurements.

3. Results

3.1. The growth of V on polycrystalline Rh at room temperature

In Fig. 1 the peak-to-peak heights of the main rhodium Auger signal at 300 eV (Rh_{300}) and of the main vanadium signal at 468 eV (V_{468}) are plotted as function of the calibrated amount of vanadium deposited at room temperature. The dotted lines in Fig. 1 are linear least-square fits to the data below 0.6 ML V coverage and between 1 and 2 ML V coverage, respectively. The solid lines are exponential fits to all data points. The nonlinear decrease (Rh), respectively increase (V), agrees with a statistical growth of simultaneous multilayers (SM), closely related to, but not as perfect as, Frank–van der Merve growth [10]. This implies that the n atom layer starts to grow before the $(n-1)$ layer is completed and can be modeled by assuming a low mobility of the adsorbate atoms on the surface. A simple calculation shows that for a nominal coverage of 1 ML 75% of the first layer, 20% of the second layer, and 5% of the third layer are filled. The inelastic mean free path of the Auger electrons is obtained by exponential data fit and compared to tabulated values. For Rh_{300} this analysis yields 8.6 Å and for V_{468} 12.2 Å, compared to 8.8 Å, respectively 11.9 Å, in the literature [14]. Thus a good agreement of fitted data and experimental points is observed assuming a SM growth. The SM growth model is also consistent with the STM investigation of vanadium on Rh(111) [8]. A similar growth mode was previously reported for vanadium on Cu(100) at RT [15] and on Cu(001) [16]. In contrast, a layer-by-layer growth was observed for vanadium on ruthenium surfaces at room temperature [17], for vanadium on W(110) [18], and for cerium on rhodium [19]. Therefore, after deposition at room temperature vanadium remains *on top* of the Rh surface and the SM growth mode determines the initial surface roughness.

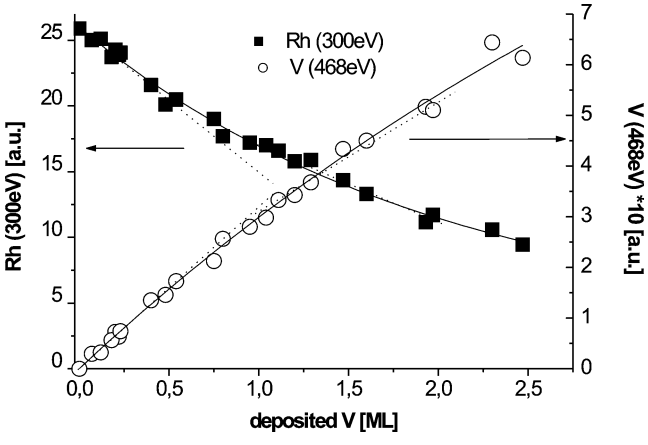

Fig. 1. Auger signals Rh_{300} and V_{468} as a function of monolayer equivalents vanadium deposited at room temperature.

3.2. Changes of the overlayer due to annealing

3.2.1. Auger spectroscopy

Annealing the vanadium overlayer caused substantial changes of the respective Auger signals. Fig. 2 illustrates the temperature dependence of the ratio V_{468}/Rh_{300} for initial vanadium exposures between 0.4 and 2.3 ML. In the submonolayer range the decrease of V_{468}/Rh_{300} is relatively small up to about 670 K, whereas with 2.3 ML V it is more pronounced and linear, probably due to increased ordering of V on the surface. Above approximately 700 K the ratio V_{468}/Rh_{300} declines rapidly for all coverages, but the decline is less pronounced above 850 K. After annealing at and above 950 K V_{468}/Rh_{300} is nearly independent of the initial coverage. For very low vanadium coverages ($\leqslant 0.2$ ML) a significantly lower onset temperature was observed. Fig. 3 shows the ratio of V_{468} after annealing and after preparation (V_{ann}/V_{prep}) as a function of annealing temperature obtained in a series of experiments with the initial V coverage varying between 0.18 and 0.22 ML, in comparison with the data for (Rh + 0.54 ML V).

In Fig. 4 the Rh_{300} and V_{468} Auger signals are plotted vs initial vanadium coverage in the asgrown state and after annealing to three characteristic temperatures (423, 773, and 950 K). Annealing at 423 K causes only a

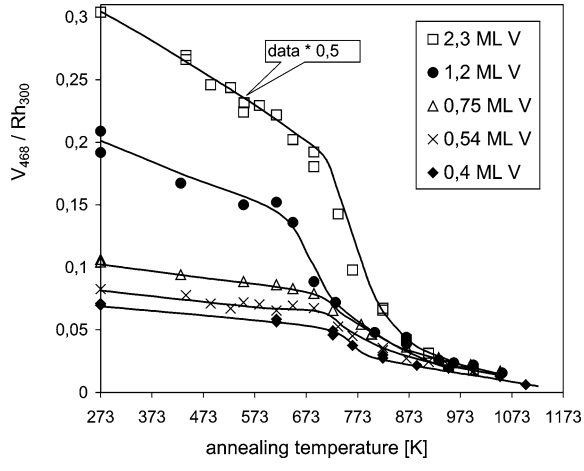

Fig. 2. Ratio of V_{468} and Rh_{300} Auger signals at different initial metal coverage as a function of annealing temperature.

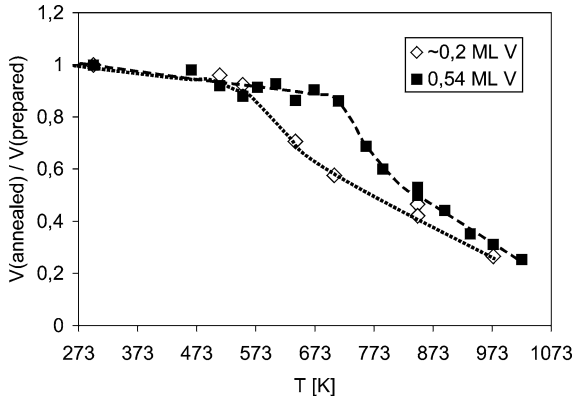

Fig. 3. Ratio of V_{468} signals after annealing and as-grown vs temperature of annealing for 0.54 and (approximately) 0.2 ML V initial coverage.

slight increase of Rh_{300} compared to the as-grown state whereas after annealing at 950 K Rh_{300} is significantly increased compared to the pristine sample (Fig. 4a). An increasing V loading causes only a small attenuation of Rh_{300}. This attenuation is linear for coverages up to 1 ML V, but above 1 ML the rhodium signal is constant and independent of the original V coverage. Finally, annealing in the midtemperature range (773 ± 30 K) also results in an increase of Rh_{300}, but the scatter of data indicates that in this temperature range small temperature variations may already have significant structural effects. However, it is clearly seen that also in this case the Rh_{300} signal first decreases and then levels off.

The corresponding V_{468} signals are depicted in Fig. 4b and show the reversed behavior. Annealing to 423 K hardly affects the vanadium concentration on the surface, but heating to 950 K causes a strong attenuation of the V signals. V_{468} increases linearly with exposure up to 1 ML and holds a constant final intensity above 1 ML. An intermediate attenuation is again observed after annealing in the temperature range close to 773 K.

Since desorption of vanadium from the surface and also its agglomeration on the surface can be excluded under the given conditions, this temperature-dependent behavior must be explained by diffusion of vanadium into the bulk. The major part of vanadium disappearing from the surface by annealing above 673 K is easily segregated back to the surface by heating in 2.0×10^{-7} mbar O_2 at 673 K, forming an overlayer of vanadium oxide, which indicates its residence in near-surface layers. Additional proof for this arises from the recent STM investigations on V/Rh(111) [8] and from the argon sputter profiles described below.

3.2.2. Argon ion sputtering

In Fig. 5 the ratio V_{468}/Rh_{300} is plotted vs sputtering time for different vanadium loadings and annealing temperatures. Fig. 5a (annealing temperature, 423 K) is representative for vanadium on top of the Rh surface as shown above: A strong decline of V_{468}/Rh_{300} is observed for the two cases of different coverage (time constant about 25 min for a decrease to $1/e$), and the sputtering time to obtain a V-free surface depends on the coverage.

Fig. 5b shows the variation of V_{468}/Rh_{300} with sputtering time of samples with V coverage below 0.5 ML annealed at 773 K. V_{468}/Rh_{300} declines with time, but the compositional changes are smaller during the initial sputter erosion and the decrease is slower compared to the samples annealed at 423 K. After very long sputtering the V signal is negligible. As already shown in Figs. 2 (e.g., 0.4 ML V) and 3, annealing at 773 K causes a substantial reduction of the V surface concentration for coverages below 0.5 ML V, and the sputter profiles conclusively indicate the diffusion of V below the surface.

Fig. 5c represents the behavior after annealing at 950 K, where V_{468}/Rh_{300} is initially identical on the two samples loaded with 1.1 and 2.3 ML vanadium, respectively. Upon sputter erosion V_{468}/Rh_{300} passes a flat maximum (after 30 min) before decreasing rapidly (after 60 min) and finally leveling off slowly. Even after prolonged sputtering vanadium is detectable. In Fig. 4a it was shown that a saturation state is reached above 1 ML V corresponding to a coverage (better exposure)-independent (sub)surface

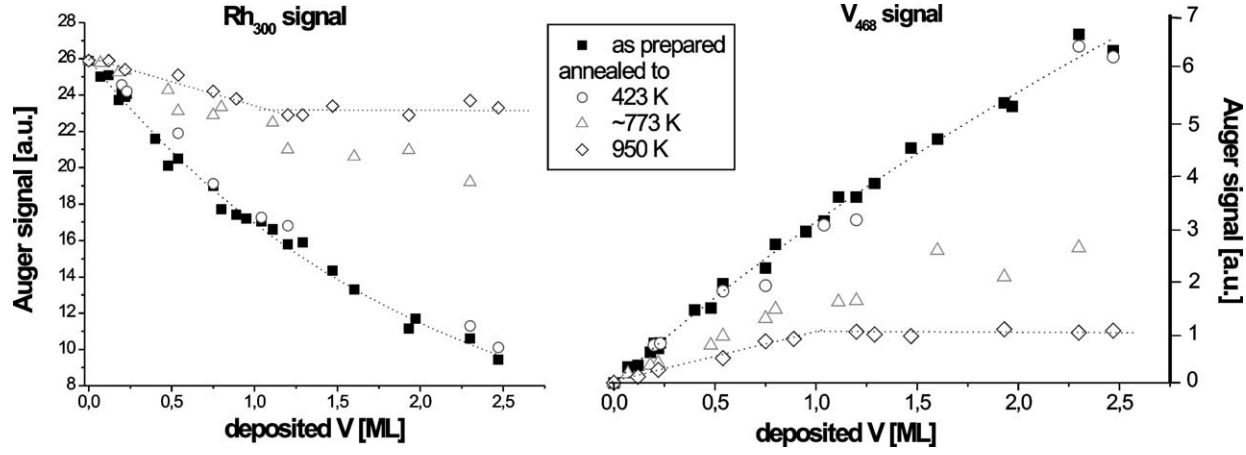

Fig. 4. Rh_{300} and V_{468} Auger signals as a function of initial coverage immediately after deposition and after annealing to 423, ~773, and 950 K.

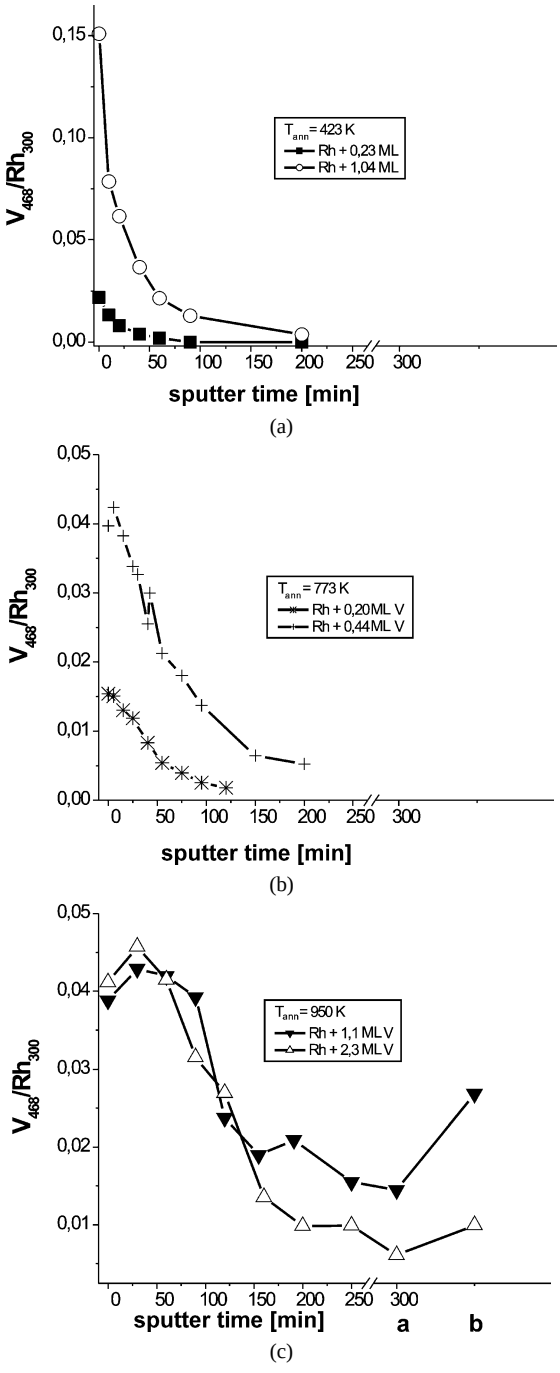

Fig. 5. V_{468}/Rh_{300} as a function of sputtering time for different initial coverage and after annealing at different temperatures (**a**, after annealing in 2.0×10^{-7} mbar H_2 at 873 K for 10 min; **b**, after heating in 2.0×10^{-7} mbar O_2 at 673 K for 10 min).

composition. The identical sputter profiles indicate that the V concentration and the in-depth extension of the subsurface layers are indeed independent of the initial coverage. The different V_{468}/Rh_{300} levels after longer sputtering reflect the different initial vanadium loading, indicating that below the saturated subsurface region excess V is accommodated in the Rh bulk. Postannealing in vacuum or in 2.0×10^{-7} mbar H_2 at 873 K has only a minor influence on the surface composition (indicated by **a** in Fig. 5c), but exposure to oxygen at 673 K leads to considerable backsegregation of vanadium to the surface and formation of a vanadium oxide overlayer (indicated by **b** in Fig. 5c) [20].

Morphologic effects and compositional changes due to different sputter yields require a calibration of the measured intensity profiles to allow a quantitative conversion into concentration profiles (concentration vs depth) [21]. Discussing the results obtained from AES one has to keep in mind that the intensity of the Auger signal contains contributions from the first 3–5 layers and therefore an averaged information within this depth, while the chemical reactivity is affected by the two topmost layers only.

In conclusion, the sputter profiles shown in Fig. 5 in combination with the temperature-dependent surface composition (Figs. 2–4) show how the in-depth distribution of V depends on the annealing temperature. After annealing at 423 K V is still on top of the surface and therefore quickly removed by sputtering. After annealing at 773 K a pronounced attenuation of the initial V_{468}/Rh_{300} ratio was observed below 0.5 ML V coverage. (These samples exhibit a high catalytic activity as will be shown in the next paragraph.) The compositional changes in the surface region upon sputtering are slower compared to vanadium on top, and V_{468}/Rh_{300} decreases until V is removed from the subsurface layers. After annealing surfaces with more than one ML V at 950 K a strong attenuation of V_{468} and a constant V_{468}/Rh_{300} were observed ("saturation"). Sputtering shows that in the near-surface layer(s) the composition varies only slightly, but that thereafter V_{468}/Rh_{300} decreases strongly and finally levels off. This indicates that the two samples in Fig. 5c are characterized by subsurface layer(s) of the same composition and thickness, while the following layers accommodate vanadium migrating from the surface into the bulk Rh.

The sputter experiments after annealing at 950 K exclude the formation of the known V/Rh bulk alloys with a composition between V_3Rh and VRh_3, as well as the *immediate* formation of a bulk solution. If a homogeneous V_xRh compound would be formed, the thickness of the new phase would increase with increasing vanadium exposure. The sputter profiles for high initial coverages, i.e., 1.1 ML V and 2.3 ML V, are identical in the beginning, indicating that both samples have the same near-surface composition. However, the different vanadium content observed in the bulk layers after prolonged sputtering reflects the different initial loading. Hence, the subsurface layers always accommodate the same amount of vanadium but a higher initial vanadium coverage leads to a higher V concentration in the Rh bulk.

3.3. Kinetic measurements

3.3.1. Kinetics on and deactivation of the bare Rh surface

The activity of the clean rhodium surface was determined repeatedly at 573 K for the "standard" CO/H_2 reactant mixture (40 mbar CO, 360 mbar H_2, He added to 1 bar). The experiments were repeated with a different Rh foil, resulting

Table 1
Activity and selectivity of the bare Rh surface as a function of $p(CO)$ and $p(H_2)$ at 573 K (He added to 1 bar total pressure)

$p(CO)$ (mbar)	$p(H_2)$ (mbar)	TOF $\times 10^2$	Selectivity (%)					Conversion[a] (%)
			Methane	Ethane	Ethene	Propane	Propene	
10	360	12.5	98.8	1.2	0	0.2	0	33.3
20	360	9.3	97.3	2.4	0	0.3	0	8.2
40	360	7.9	98	2	0	0	0	4.8
40	360	7.6	96.9	3	0	1	0	6.1
70	360	6.4	91.5	8.2	0.30	1.3	0	0.3
100	360	6.2	85.2	8.9	0.3	1.8	3.7	3.8
40	120	1.7	96.7	3.2		0.1		2

[a] Conversion at which the selectivity was determined.

Table 2
Activity and selectivity of the bare Rh surface as a function of reaction temperature. Reaction conditions: 40 mbar CO, 360 mbar H_2, 600 mbar He

T[a] (K)	TOF (1/(s site))	Selectivity (%)					Conversion[b] (%)
		Methane	Ethane	Ethene	Propane	Propene	
471	0.00060	75.8	13.1	5.5	5.6		0.17
522	0.016	89.2	9	0.7	1.4		0.17
548.5	0.030						
573	0.078	96	4				1.04
599	0.24						
623.5	0.39	98.7	1.3				19.0

[a] Corrected sample temperature.
[b] Conversion at which the selectivity was determined.

in exactly the same reaction rates (±5%) and selectivities under the same reaction conditions.

Activity and selectivity data for varying CO and H_2 partial pressures at 573 K are summarized in Table 1. The reaction orders in CO and hydrogen were deduced from the *initial TOF*. Reaction orders of −0.31 for CO and of 1.14 for H_2 were determined, in good agreement with Vannice [22] and Logan and Somorjai [23]. At low conversion the product formation increases linearly with time, but at high conversion some deactivation is observed, especially at a high CO/H_2 ratio. Auger spectra recorded after reaction reveal the presence of carbon and oxygen. The oxygen-containing species, mainly CO, are removed from the surface below the detection limit by heating in vacuum near 600 K. The Auger spectra recorded after different reaction times and subsequent flashing at 623 K reveal that C_{270}/Rh_{300} initially increases and reaches a nearly constant level, corresponding to a steady-state concentration of surface carbon. This steady-state concentration increases almost linearly with the CO/H_2 ratio, but it is always below 1 ML. Only a small fraction (5–20%) of the carbon deposited during reaction reacts subsequently with hydrogen at 573 K while the rest will block the surface and decrease the active area. Contrary to adsorbed carbon, adsorbed oxygen does not influence the kinetic results, since it is easily removed with hydrogen at and above 373 K.

In Table 2 the temperature dependence of the activity and selectivity of CO hydrogenation on the bare Rh surface are shown. From an Arrhenius plot taken between 470 and 623 K an apparent energy of activation of 102 ± 5 kJ/mol was determined for a $CO:H_2$ ratio of 1:9, in very good agreement with previous work [11,22,23].

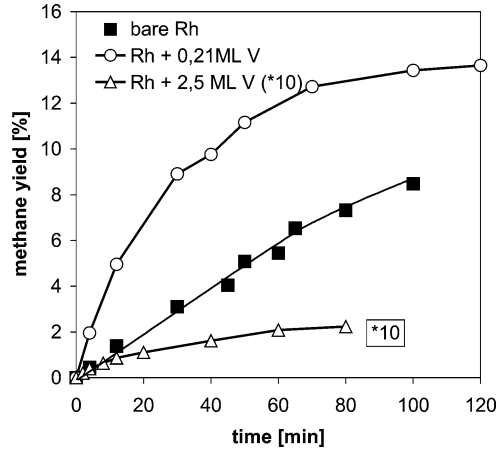

Fig. 6. Methane yield vs time on the bare Rh surface and on a surface covered with 0.21 and 2.5 ML V after heating to 423 K. Reaction conditions: 40 mbar CO, 360 mbar H_2, 600 mbar He, 573 K.

3.3.2. Vanadium metal-modified rhodium surfaces

3.3.2.1. After annealing to 423 K. As shown before, in this state the system is still a true vanadium metal overlayer on top of rhodium. The presence of vanadium on the surface is also evident from the analysis of the surface composition after reaction.

In Fig. 6 the methane production is shown as a function of reaction time for (Rh + 0.21 ML V) and (Rh + 2.5 ML V, data multiplied by 10), compared to bare Rh. The reaction conditions were 40 mbar CO, 360 mbar H_2, and 600 mbar He at 573 K. With submonolayer deposits of vanadium the initial activity is higher than on the bare rhodium surface, but the catalyst deactivates rapidly (the TOF drops by a factor of 20 after the initial promotion). The selectivity toward methane is initially 73% and increases slightly to 78%. For (Rh + 2.5 ML V) the *initial TOF* is more than an order of magnitude smaller than on the bare Rh surface and decreases further with time to about $\frac{1}{2}$ of the initial value. The methane selectivity is then about 68%. Hence, an *initial* promotion of CO hydrogenation occurs only for very low vanadium coverage, but strong deactivation limits the promotion to the initial phase of the reaction. The postreaction Auger

spectra of Rh surfaces with high vanadia loading reveal large amounts of carbon and oxygen, while the vanadium and rhodium signals are strongly attenuated. Heating to 483 and 573 K leads to a reduction of the carbon signal, but no significant change in the oxygen signal. On the other hand, heating to 700 K leads to significant changes in the Rh and V signals, while the O signal is reduced and the C signal is more "symmetric."

The results can be understood on the basis of the reactivity of metallic vanadium. Like all early transition metals vanadium adsorbs and dissociates CO. The resulting oxygen and carbon species are strongly bound to the surface. A reduction of vanadium oxide at reaction temperature is not feasible. Oxygen adsorbed on vanadium single-crystal surfaces cannot be removed as water by dosing hydrogen molecules or atoms [24] but may be dissolved in the vanadium bulk. Vanadium carbides also have a low reactivity toward hydrogen. Although pure vanadium metal adsorbs hydrogen and may even form stable bulk hydrides, hydrogen dissociation does not occur on vanadium oxide and vanadium carbide surfaces. Thus the main reaction paths for methane formation are blocked.

It is reasonable to assume the conversion of vanadium metal to vanadium oxide/carbide also on submonolayer deposits of vanadium. Postreaction Auger spectra of (Rh + 0.21 ML V) indicate that the vanadium concentration on the surface remains essentially unchanged during the reaction. The carbon peak is less intense and more symmetric than in the case of "thick" vanadium overlayers. The oxygen content of the surface is slightly higher than on bare rhodium after reaction. However, oxygen can be removed to a level below the detection limit of AES by heating in vacuum to 573–623 K, while the carbon signal is more or less unaffected. Oxygen adsorption seems to be affected by dissociated hydrogen spilt over from bare Rh patches, and O is therefore less strongly bound than on thick vanadium layers and also than oxygen in a VO_x adlayer. Hence in this case vanadium metal is not fully oxidized to V_2O_3 under reaction conditions, but species like vanadium oxicarbide are formed during the reaction, like on "thicker" V overlayers on Rh. In this case, the deactivation with reaction time is again accompanied by an increasing deposition of carbon on the surface.

3.3.2.2. After annealing at 773 K. An annealing temperature of 773 K is above the onset of vanadium diffusion, but still in the dynamic range where V_{468}/Rh_{300} depends strongly on T (Fig. 2). In Fig. 7 conversion vs time is plotted for a number of different initial loadings. The reaction conditions were again 40 mbar CO, 360 mbar H_2, and 600 mbar He at 573 K. In this series the highest activity is observed for (Rh + 0.46 ML V). Generally, on samples with low initial vanadium coverage (< 0.5 ML) the methane yield increases linearly up to high conversion, indicating slow deactivation. For higher vanadium coverage the activity decreases more significantly with increasing time. The strong rate enhancement by a small added amount of vanadium indicates that one vanadium atom must affect more than one rhodium site.

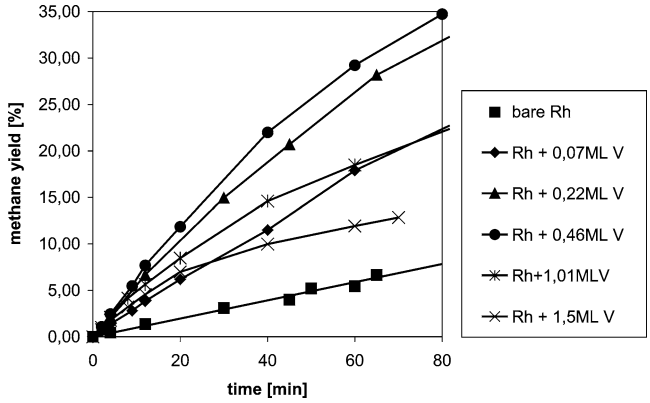

Fig. 7. Conversion vs time for (Rh + x ML V) annealed to 773 K in 2.0×10^{-7} mbar H_2 for 10 min. Reaction conditions as in Fig. 6.

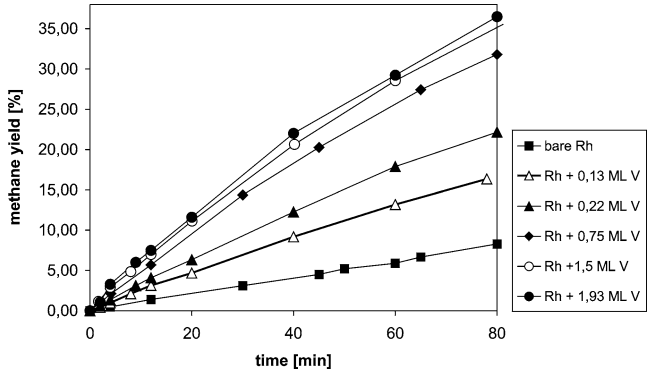

Fig. 8. Methane production vs time on (Rh + x ML V) annealed to 950 K. Reaction conditions as in Fig. 6.

The postreaction Auger spectra of samples annealed at (approximately) 773 K show that on samples with initial loading up to about 0.5 ML V the carbon and oxygen contents are low and about the same as on the bare Rh surface. If the initial V loading exceeds 0.5 ML they both increase with vanadium coverage. Thus, the deactivation observed on samples with coverage above 773 K is accompanied by carbon formation and oxygen deposition on the surface similar to what is observed with V on top of the surface. On the other hand, the temperature-dependent evolution of surface composition shown in Figs. 2 and 3 and the sputter profiles in Fig. 5b demonstrate that below 0.5 ML the material transport is already completed and the surface is covered by a Rh skin. The low carbon and oxygen content of these postreaction surfaces and the reduced deactivation during reaction are also in agreement with the absence of on-top vanadium.

3.3.2.3. After annealing to 950 K. The compositional changes induced by annealing to 950 K have already been discussed in [10] and in Section 2.2.1. In Fig. 8 conversion vs time is plotted for a number of different initial loadings, again under the same reaction conditions (40 mbar CO, 360 mbar H_2, 600 mbar He at 573 K). Conversion vs

Table 3
Activity and selectivity of (Rh + x ML V) annealed at 950 K

Sample	TOF	Selectivity (%)				
	(1/(s site))	Methane	Ethane	Ethene	Propane	Propene
Bare Rh	0.076	97.5	2.5			
Rh + 0.12 ML V	0.13	88.9	8.2	0.2	1.3	1.4
Rh + 0.17 ML V	0.20	89.1	8.0	0.1	1.5	1.3
Rh + 0.4 ML V	0.25	87.5	9.9	0.1	1.5	0.9
Rh + 0.75 ML V	0.35	88.9	8.9	0.1	1.2	0.9
Rh + 1.2 ML V	0.37	87.4	10.4	0.1	1.4	0.7
Rh + 1.3 ML V	0.39	85.2	11.9	0.3	2.2	0.4
Rh + 2.0 ML V	0.38	86.9	11.1		1.8	0.2

Reaction conditions: 40 mbar CO, 360 mbar H^2, 600 mbar He, 573 K.

time plots are linear up to high conversion (depending on the reaction conditions) for all initial coverages, indicating very little deactivation. The dependence of activity and selectivity on the initial V coverage is summarized in Table 3. While the TOF increases with coverage up to about 1 ML and remains constant thereafter, the selectivity undergoes only minor changes. According to the Auger spectra the carbon content of all surfaces is low and comparable to the bare rhodium surface after reaction under identical conditions. Likewise, the oxygen content is similar or only slightly higher than on bare rhodium after reaction. In contrast to annealing to 773 K no appreciable change with increasing vanadium content is observed.

The kinetic parameters were determined for a V/Rh surface with 1.2 ML initial V coverage and annealing at 950 K. Their dependence on the CO and H_2 partial pressure is summarized in Table 4. The reaction orders were -0.34 for CO and $+1.2$ for H_2. The reaction rate (as well as the selectivity toward methane) is increased either by decreasing p(CO) at constant $p(H_2)$, or by increasing $p(H_2)$ at constant p(CO). Table 5 summarizes the *initial TOF* and the selectivity of (Rh + 1.2 ML V) under standard reaction conditions (40 mbar CO, 360 mbar H_2, and 600 mbar He) after annealing at 950 K as a function of temperature. At 573 K the methane production is between 89 and 85%, with ethane as the most prominent minor product with 8 to 12%. However, at 471 K the selectivity toward alkanes and particularly alkenes is enhanced. Oxygenates were not detected under the given conditions. From an Arrhenius plot an activation energy of 104 ± 3 kJ/mol and a prefactor of 9.8×10^8 molecules/(s site) are obtained.

4. Discussion

4.1. Formation and properties of (sub)surface alloys

So far, only a small number of binary surfaces consisting of early and late transition metals have been described in the literature. The combination of electron-poor and electron-rich transition metals, with significantly different d-band occupation, leads to a strong interaction between the metals and determines the adsorption properties and the chemical reactivity of such bimetallic systems. The structure and composition of a metal overlayer on a metal surface can be understood in terms of segregation energy and mixing energy [25,26]. Depending on the sign of the segregation energy, the adsorbate will stay on the surface ($E_{\text{seg}} < 0$) or migrate into the bulk ($E_{\text{seg}} > 0$). The mixing energy determines whether an alloy ($E_{\text{mix}} > 0$) or separate phases ($E_{\text{mix}} < 0$) are formed. In principle, the behavior of metals deposited on a metal substrate can be classified into one of these four cases. However, kinetic reasons can give rise to structures differing from those predicted by thermodynamics. Both the thermal behavior of a bimetallic system and a gas phase-induced surface segregation must be taken into account. In surface alloys, the composition of successive layers may not be uniform and frequently no counterpart in bulk structures is observed; e.g., Al on Pd(111) forms bilayered island structures consisting of a Al–Pd layer covered by pure Pd [39].

Former kinetic studies on bimetallic systems have been concerned with alloys and supported bimetallic particles [27], or with pseudomorphic overlayers of active metals on dissimilar substrates [28–32]. Studies of the CO hydrogenation on alloys have been reviewed by Ponec [33] who distinguished bimetallic catalysts with either both components remaining in the zero valent state during reaction or one component converted to oxide or carbide by the reactants. In the second case the contributions of the second metal can be discussed as promoter effects. If an active metal is combined with an inactive metal the activity is usually related to the ensemble size of the active component [34]. Rodríguez and Goodman [35] showed that pseudomorphic overlayers of Ni, Pd, and Cu on a dissimilar substrate (Ta, W, Re, Ru, Mo) exhibit a different reactivity than the pure metal. They correlated the CO chemisorption energy to the surface core level

Table 4
CO hydrogenation on (Rh + 1.2 ML V) annealed at 950 K, dependence on p(CO) and $p(H_2)$

p(CO)	$p(H_2)$	TOF	Selectivity (%)					Conversion[a]
(mbar)	(mbar)	(1/(s site))	Methane	Ethane	Ethene	Propane	Propene	(%)
10	360	0.48	96	3.7		0.3		38
40	360	0.37	85	12.0	0.4	2.0	0.6	14
70	360	0.27	75.8	15.7	2.3	2.2	4.0	4.5
100	360	0.25	70.8	16.2	4.1	2	6.9	2.6
40	120	0.16	69	13.2	7.6	1.7	8.5	1.3

Reaction temperature 573 K.
[a] Conversion at which the selectivity was determined.

Table 5
Activity and selectivity of the V/Rh subsurface alloy (1.2 ML V, annealed at 950 K) as a function of reaction temperature

T[a]	TOF	Selectivity (%)					Conversion[b]
(K)	(1/(s site))	Methane	Ethane	Ethene	Propane	Propene	(%)
471	0.0028	51.4	16.2	18.3		14.0	0.44
522	0.030	75.1	18.5	3.3	3.0		
548.5	0.12						
573	0.36	85.2	11.9	0.3	2.2	0.4	14
599	0.70	98.1	1.5		0.4		42.3
623.5	1.85	100					87.8

Reaction conditions: 40 mbar CO, 360 mbar H_2, 600 mbar He.
[a] Corrected sample temperature.
[b] Conversion at which the selectivity was determined.

shifts observed by XPS. In a theoretical investigation Hammer and co-workers [36,37] concluded that the modified reactivity of the overlayer can be explained by the position of the center of the metal d-band, and reproduced the experimental results successfully. Ruban et al. [38] calculated and tabulated the shift in the d-band center for a number of metal overlayers on metals and for metal surfaces modified by dissimilar metal adatoms.

In the V/Rh system (and in the related V/Pd system) the catalytically active noble metal is combined with vanadium, which reacts with CO toward oxides and carbides. Pure vanadium dissociates CO and the resulting oxygen and carbon species are firmly bound to the surface. Due to this self-poisoning the vanadium surface and the V-covered Rh surface are inactive in CO hydrogenation (see Fig. 6). Submonolayers of V are also modified during reaction by the formation of vanadium oxide and/or carbide compounds. The composition of these compounds, however, differs from pure vanadium oxide overlayers [20]. The initial promotion by surface V can be related either to V metal initially present on the surface or to the oxidized vanadium compound formed during reaction.

The surface composition of the V/Rh system undergoes significant changes upon annealing. E_{seg} and E_{mix} are positive for vanadium on palladium and rhodium, and alloy formation is predicted. In fact, several stable rhodium–vanadium bulk alloy phases are known. The subsurface alloy phases are best described as kinetically stable intermediates on the way toward alloy formation. The structural properties of V/Pd and V/Rh subsurface alloys on (111) Rh surfaces are now well known. On Pd(111) Varga and co-workers [6] observed the formation of a surface alloy and of a subsurface alloy, depending on the substrate temperature. The topmost layer of the subsurface alloy consists of Pd atoms and in the second layer every third Pd atom is replaced by vanadium, yielding a Pd surface structurally and electronically modified by subsurface vanadium. Density-functional theory calculations [6,7] confirmed the tendency of vanadium for heterocoordination by substitution with surface atoms or migration into near-surface layers, both driven by the formation of strong V–Pd bonds. Vanadium atoms in the second layer are thermodynamically more stable than vanadium atoms on the surface or in the bulk. The stability in the second layer is associated with the fact that vanadium gains more electron density from the coordinatively unsaturated surface atoms than from atoms with bulk coordination. The adsorption properties of V–Pd alloys were investigated by Beutl and co-workers [40,41] and by Surnev et al. [42]. Both hydrogen and CO desorption peaks are shifted to lower temperatures, indicating a lower desorption energy of the two gases on the alloy surface. As on Pd surfaces, but in contrast to vanadium surfaces, CO dissociation does not occur on the alloy surface. CO dissociation occurs, however, after deposition of vanadium on Pd at low temperatures.

The V/Rh subsurface alloy is formed analogously from vanadium overlayers on Rh(111) [8], but at somewhat higher temperature. The temperature needed for alloy formation from metal overlayers is approximately 523 K for Pd(111) and about 823 K for Rh(111) (compared to 773 K on polycrystalline Rh). The difference arises from the higher cohesive energy of rhodium; thus higher temperatures are required than on palladium to achieve sufficient mobility of the substrate atoms. On Rh(111) the subsurface alloy exhibits a (2×2) structure and is saturated with 0.25 ML V in the subsurface layer. Hence, the structure of the V/Rh intermetallic compound on *polycrystalline* Rh may be interpreted in view of the thoroughly investigated (sub)surface alloy of vanadium on Pd(111) [6,7] and the similar (sub)surface alloy on Rh(111) [8].

The polycrystalline Rh surface is of course more complex than Rh(111). It contains facets of close-packed planes and more defects like step edges and grain boundaries. The high number of defects will influence the formation and morphology of a V/Rh intermetallic compound. In principle several mechanisms are conceivable: a dissolution of vanadium in the rhodium bulk starting at defect sites like steps, grain boundaries, etc., or a diffusion of rhodium into the vanadium layers and growth of a surface alloy on top of the rhodium substrate. The STM investigations on the analogous V/Pd(111) system have revealed details about the growth mechanism of the alloy [6]. Due to the mass transport between V and Pd both the atomic roughness and the dimensions of the step edges on the surface increase. While on the flat single-crystal surface the growth of the subsurface alloy appears to start mainly from step edges, a growth from the grain boundaries is more likely in the present case. The average Rh grain size has remained constant over the full period of our experiments and it seems that the subsurface alloy growth always ends in reproducible structures.

4.2. Rh/V: composition and catalysis after annealing to three different temperatures

The experimental results can be divided into three cases, according to the temperature of annealing. Fig. 9 shows the overall activity as a function of initial exposure after annealing to three characteristic temperatures (423, 773, and

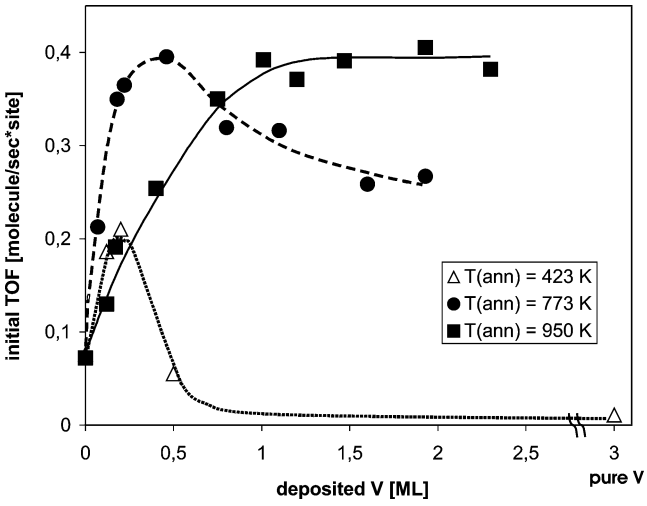

Fig. 9. Initial turnover rates as a function of initial vanadium exposure after annealing at 423, 773, and 950 K for 10 min. Reaction conditions as in Fig. 6.

950 K). Selectivity changes are summarized Tables 3, 4 and 5.

After deposition at room temperature the surface composition changes only slightly upon annealing up to reaction temperature (573 K), except for very low coverage. Vanadium remains on the surface and only small amounts ($\ll 0.2$ ML) are incorporated into defects at the surface. A completely V-covered surface is not active for CO hydrogenation due to the reasons described above, while submonolayers of V on the surface lead to an (only) initial promotion of the CO hydrogenation (Figs. 6 and 9). The postreaction Auger spectra of these surfaces show a significantly higher carbon and oxygen content after reaction compared to bare Rh or to V/Rh alloy. Vanadium reacts with CO and hydrogen and in addition with the reaction product water. Thus, the vanadium metal overlayer is converted to a complex system containing vanadium oxide and carbide, or even hydride. The initial promotion might be either due to an influence from the initially pristine V metal or due to vanadium oxide/carbide formed during reaction. Bare rhodium patches dissociate hydrogen and supply atomic hydrogen for the hydrogenation of carbon on rhodium and/or the hydrogenation of vanadium carbide. A common distinctive feature of V on top of Rh is the strong deactivation with increasing time. This deactivation is not observed for V/Rh alloy samples.

After heating to 950 K the composition of the surface and subsurface layer is uniform for initial coverages above 1 ML V (Fig. 4). For exposures in excess of 1 ML the same V_{468}/Rh_{300} ratio (0.04 ± 0.003) is observed and in addition a constant catalytic activity is observed above 1 ML (Fig. 9). The postreaction spectra of V/Rh annealed at 950 K show that the carbon content increases slightly with increasing vanadium coverage, but is still low compared to a surface with "0.2 ML V on top of Rh." Furthermore, the conversion vs time plots indicate only little deactivation (Fig. 8). This is consistent with the assumption that the concentration of vanadium in the topmost surface layer is zero, or at least very low. If this strong promotion would arise from vanadium remaining *on* the surface at low concentration, it would have to be observed on low-coverage samples annealed to lower temperatures as well, which is not the case. Hence it must be concluded that only vanadium in the near-surface region is involved in the mechanism. The sputter profiles after annealing to 950 K (Fig. 5c) showed that samples with initial coverage above about 1 ML V have an equal composition of the near-surface layers, and that also the "thickness" of the V/Rh compound is independent of the initial coverage. The onset of subsurface migration of V is already observed after annealing coverages below 0.5 ML at 773 K (see below). However annealing at 950 K facilitates the dissolution of V in the Rh bulk, thereby excluding the presence of surface V, while saturation of the subsurface layer is still achieved. Finally, annealing at even higher T (1073 K) destabilizes the subsurface layer and V diffuses into the bulk.

Samples annealed at 773 K exhibit a more complex dependence of the catalytic activity on the V exposure (Fig. 9). The CO hydrogenation activity increases strongly up to about 0.5 ML V and decreases gradually thereafter. Figs. 3 and 4 (0.4 ML) show that a significant surface modification already occurs in the low coverage range upon annealing at 773 K. It seems that at 773 K the interdiffusion between vanadium and rhodium is kinetically limited. A saturation of the subsurface layer occurs between 0.25 and 0.5 ML V and for coverages in excess of 0.5 ML vanadium remains partly on the surface because the transition from the second to the following layers (to the bulk) is hindered. On the basis of the postreaction spectra, samples annealed at an intermediate temperature can also be divided into two groups. Surfaces with equal or less than 0.5 ML V initial coverage exhibit linear conversion vs time plots (Fig. 7) and a low carbon level after reaction, whereas for initial coverage above 0.5 ML V a higher and increasing carbon concentration is observed. The presence of excess vanadium on the surface together with the associated accumulation of carbon also accounts for the gradual activity decline with reaction time.

Hence, the optimum performance will be obtained by adapting the subsurface composition—by varying either the amount of vanadium or the annealing temperature. For example, a sample with $V_{468}/Rh_{300} = 0.04$ can be prepared by depositing more than 1 ML V and annealing to 950 K, or by depositing 0.5 ML V and annealing to 773 K (Fig. 9). The catalytic activity of the two samples is identical (~ 0.39 molecules/(s site)) and the conversion vs time plots are both linear. Samples with less than 0.2 ML V annealed at 773 K have already a high activity, i.e., a high V concentration (near saturation) in the second layer. However, annealing at higher temperature (e.g., 950 K) will lead to partial dissolution in the bulk and to a decreased vanadium concentration in the subsurface layer. In fact, Varga and coworkers [8] observed the saturation of the subsurface layer on V/Rh(111) at 0.25 ML V. On polycrystalline Rh we

may assume a V/Rh stoichiometry 0.25 to 0.3 in the second layer. Thus it is reasonable to relate the maximum activity enhancement to the saturation of the subsurface layer with vanadium. Vanadium in the second (subsurface) layer is kinetically stable in the "intermediate" temperature regime around 773 K. Between 900 and about 1000 K the second layer is still kinetically stable, but additional V monolayers can be dissolved in the Rh bulk without influencing further the catalytic activity. At 1050 K the diffusion of V into the bulk is predominant and the promotional effect disappears.

The reaction orders, measured in the saturation coverage range (-0.34 for CO and $+1.2$ for hydrogen) were almost unchanged with respect to the bare Rh surface. Also the apparent activation energy of 103 ± 5 kJ/mol was almost identical. Hence, the sixfold rate increase at maximum must be interpreted as a sixfold increase of the preexponential factor.

Chemisorption studies on the Pd(111) [40–42] and Rh (111) [43] subsurface alloys reveal dramatic changes relative to the clean metal surface. The reactivity of the pure metal surfaces and also of the two subsurface alloys toward CO dissociation is very low. Measurable CO dissociation does not occur within the pressure and temperature range covered by surface science techniques. Measurements of sticking probabilities and photoemission data indicate a reduction of the room-temperature saturation coverage to about 50% on the Rh/V alloy surface [43]. On both Pd/V and Rh/V the thermal desorption peak of CO is shifted to significantly lower temperature. This decrease up to 70 K depends on the vanadium content of the subsurface layers and indicates a significant decrease of the CO binding energy. On V/Pd(111) also the sticking coefficient and the desorption energy of hydrogen are decreased by alloy formation, though less dramatically [42].

Since the reaction order in CO is negative and CO inhibits the reaction, the activity increase by added vanadium might be explained by a decreased coverage of CO compared to hydrogen, resulting in an increased reaction rate according to a Langmuir–Hinshelwood scheme. As also discussed in [10], this explanation is probably not satisfying because the changes of the reaction kinetics from the clean Rh surface to the subsurface alloy are limited to an increase of the preexponential factor in the Arrhenius equation, and because it does not account for the changing surface morphology during alloy growth. Defects, especially step edges, are believed to play a dominant role for the dissociation of CO. It has been shown earlier that on rhodium CO dissociation occurs only on stepped and defect-rich surfaces [44] and it is also known that the rate of CO hydrogenation is enhanced on a defect-rich Rh(111) surface [9]. If we consider the mode of subsurface alloy growth which involves the transport of Rh on top of the surface, the number of step edges on the surface, available as reactive sites for CO dissociation, will increase [6,8]. The observed *reproducible* rate increase at a given surface composition may be explained by the reproducible V-induced formation of structures with a high but constant number of step edge sites. This must be proved in a separate STM experiment on a single-crystal Rh surface.

Finally, the selectivity of the subsurface alloy is closely related to its activity (Tables 3, 4, and 5). Although in these experiments the reaction kinetics was always measured in excess hydrogen it is obvious that the subsurface alloy is more selective toward longer chain hydrocarbons than the clean Rh metal surface, but less selective than submonolayers of vanadia on Rh [20]. Taking into account that subsurface vanadium attracts electrons from the Rh surface, one may explain the properties of the alloy surface as resembling those of ruthenium metal, the left neighbor of Rh in the periodic table, which is known for a higher methanation activity and also a higher selectivity toward alkanes than Rh. As a whole, the effect of subsurface vanadium on the catalytic properties can be interpreted as twofold: an electronic part (ligand effect), caused by the attraction of electrons from the Rh surface atoms, and a structural part, due to the vanadium-induced reproducible concentration of step edges. A proof of this hypothesis is a challenge for a future STM investigation in which specific subsurface alloy structures are formed on a single-crystal surface with known subsurface composition, and the kinetics on these surfaces is measured.

5. Conclusions

We have investigated the composition, structure, and kinetic properties of V/Rh system under varying preparation conditions. V overlayers on top of the surface are observed after deposition of V at room temperature and are predominant for annealing temperatures below 573 K. At small coverages surface V leads to an initial promotion of the CO hydrogenation; however, a strong deactivation caused by carbon formation and conversion of the V metal to vanadium oxide/carbide compounds is observed. Thus surface vanadium does not remain in its metallic state during reaction.

Extensive compositional changes are observed after annealing above 773 and 950 K and the surface and subsurface composition depends markedly on the V exposure and the annealing temperature. Annealing at 773 K facilitates the incorporation of V in subsurface layers; thus by annealing at this particular temperature a vanadium amount equal or close to subsurface saturation (between 0.25 and 0.5 ML on polycrystalline Rh) is accommodated in the subsurface layer. The V/Rh subsurface alloy exhibits a high catalytic activity even with small subsurface concentrations of V, with negligible deactivation and a modified selectivity. For higher V exposures some excess V remains on the surface after annealing at 773 K, leading to a gradual activity decrease.

Increasing the annealing temperature to 950 K still leads to a saturation of the kinetically stable subsurface layer, but also facilitates the dissolution of excess V in the Rh bulk. The subsurface layer is filled up to an initial exposure of about 1 ML (some dissolution into the bulk might occur simultaneously) and for higher initial exposures a constant

composition is then obtained. Similar to the evolution of the composition also the activity increases up to 1 ML V and remains constant as soon as the subsurface layer is saturated (and excess V is dissolved in the bulk).

The observed promotion into the highly active state is related to the formation of the subsurface alloy consisting of a noble metal Rh surface skin electronically modified by the dissimilar zero valent metal in the second layer. The alloy formation is also accompanied by morphological changes. For highest activity and accompanying low catalyst deactivation a saturated subsurface layer and a vanadium free surface are necessary, achieved by adjusting the initial V exposure and the annealing temperature.

Acknowledgment

This work was supported by the Austrian Science Fund (Project S 8105).

References

[1] C.T. Campbell, Annu. Rev. Phys. Chem. 41 (1990) 775.
[2] J.A. Rodríguez, Surf. Sci. Rep. 24 (1996) 223.
[3] G.A. Somorjai, Introduction to Surface Chemistry and Catalysis, Wiley, New York, 1994.
[4] J.H. Sinfelt, Bimetallic Catalysts, Wiley, New York, 1983.
[5] V. Ponec, Adv. Catal. 32 (1983) 149.
[6] C. Konvicka, Y. Jeanvoine, E. Lundgren, G. Kresse, M. Schmid, J. Hafner, P. Varga, Surf. Sci. 463 (2000) 199.
[7] R. Hirschl, Y. Jeanvoine, J. Hafner, J. Phys. Condens. Mater. 13 (2001) 3545.
[8] C. Konvicka, PhD thesis, Technical University of Vienna, 2002;
C. Konvicka, W. Rupp, M. Schmid, P. Varga B. Klötzer, K. Hayek, in preparation.
[9] K. Hayek, B. Jenewein, B. Klötzer, W. Reichl, Top. Catal. 14 (2001) 25.
[10] W. Reichl, K. Hayek, Surf. Sci. 537 (2003) 247.
[11] M.E. Levin, M. Salmeron, A.T. Bell, G.A. Somorjai, J. Chem. Soc., Faraday Trans. 183 (1987) 2061.
[12] A.B. Boffa, A.T. Bell, G.A. Somorjai, J. Catal. 139 (1993) 602.
[13] W. Reichl, G. Rosina, G. Rupprechter, C. Zimmermann, K. Hayek, Rev. Sci. Instrum. 71 (2000) 1495.
[14] S. Tanuma, C.J. Powell, D.R. Penn, Surf. Interf. Anal. 17 (1991) 911.
[15] P. Pervan, T. Valla, M. Milun, Surf. Sci. 397 (1998) 270.
[16] D.P. Moore, O. Ozturk, F.O. Schumann, S.A. Morton, G.D. Waddill, Surf. Sci. 449 (2000) 31.
[17] M. Albrecht, J. Pohl, H. Wider, E.U. Malang, J. Köhler, K. Friemelt, E. Bucher, Surf. Sci. 397 (1998) 354.
[18] J. Kolaczkiewicz, E. Bauer, Surf. Sci. 450 (2000) 106.
[19] J.P. Warren, X. Zhang, J.E.T. Anderson, R.M. Lambert, Surf. Sci. 287/288 (1993) 222.
[20] W. Reichl, K. Hayek, J. Catal. 208 (2002) 422.
[21] M.P. Seah, in: D. Briggs, M.P. Seah (Eds.), Practical Surface Analysis, Wiley, New York, 1983, p. 181 ff.
[22] M.A. Vannice, J. Catal. 37 (1975) 449.
[23] M.A. Logan, G.A. Somorjai, J. Catal. 95 (1985) 317.
[24] G. Krenn, C. Eibl, W. Mauritsch, E.L.D. Hebenstreit, P. Varga, A. Winkler, Surf. Sci. 445 (2000) 343.
[25] A.V. Ruban, H. L Skriver, J.K. Norskov, Phys. Rev. B 59 (1999) 15990.
[26] A. Christensen, A.V. Ruban, P. Stoltze, K.W. Jacobsen, H. L Skriver, J.K. Norskov, Phys. Rev. B 56 (1996) 10.
[27] W.M.H. Sachtler, Faraday Disc. Chem. Soc. 72 (1981) 7.
[28] C.M. Greenlief, P.M. Berlowitz, D.W. Goodman, J.M. White, J. Phys. Chem. 91 (1987) 6669.
[29] P.M. Berlowitz, D.W. Goodman, Surf. Sci. 187 (1987) 463.
[30] B.G. Johnson, C.H. Bartholomew, D.W. Goodman, J. Catal. 128 (1991) 231.
[31] C.H.F. Peden, D.W. Goodman, Ind. Eng. Chem. Fundam. 25 (1986) 58;
C.H.F. Peden, D.W. Goodman, J. Catal. 104 (1987) 347.
[32] D.W. Goodman, in: Proc. IUCCP Conf. on Heterogeneous Catalysis, Texas A&M University, 1984.
[33] V. Ponec, in: G. Ertl, H. Knözinger, J. Weitkamp (Eds.), Handbook of Heterogeneous Catalysis, Wiley–VCH, Weinheim, 1997, p. 1876 ff.
[34] L.J.M. Luyten, M. van Eck, J. van Grondelle, J.H.C. van Hooff, J. Phys. Chem. 82 (1978) 200.
[35] J.A. Rodríguez, D.W. Goodman, Science 257 (1992) 897.
[36] B. Hammer, J.K. Norskov, Surf. Sci. 343 (1995) 211.
[37] B. Hammer, Y. Morikawa, J.K. Norskov, Phys. Rev. Lett. 76 (1996) 2141.
[38] A. Ruban, B. Hammer, P. Stoltze, H.L. Skriver, J.K. Norskov, J. Mol. Catal. A 115 (1997) 412.
[39] K. Kishi, A. Oka, N. Takagi, M. Nishijima, T. Aruga, Surf. Sci. 460 (2000) 264–276.
[40] M. Beutl, J. Lesnik, K.D. Rendulic, R. Hirschl, A. Eichler, G. Kresse, J. Hafner, Chem. Phys. Lett. 342 (2001) 473.
[41] M. Beutl, J. Lesnik, Surf. Sci. 482 (2001) 353.
[42] S. Surnev, M. Sock, M.G. Ramsey, F.P. Netzer, B. Klötzer, W. Unterberger, K. Hayek, Surf. Sci. 511 (2002) 392.
[43] B. Klötzer, W. Unterberger, K. Hayek, Surf. Sci. 532–535 (2003) 142.
[44] P.A. Thiel, W.D. Williams, J.T. Yates, H.W. Weinberg, Surf. Sci. 91 (1980) 522.